Carbon Dioxide-in-Water Foams Stabilized with Nanoparticles and Surfactant Acting in Synergy

Andrew J. Worthen
Dept. of Chemical Engineering, The University of Texas at Austin, Austin, TX 78712

Steven L. Bryant, and Chun Huh
Dept. of Petroleum & Geosystems Engineering, The University of Texas at Austin, Austin, TX 78712

Keith P. Johnston
Dept. of Chemical Engineering, The University of Texas at Austin, Austin, TX 78712

DOI 10.1002/aic.14124
Published online May 16, 2013 in Wiley Online Library (wileyonlinelibrary.com)

Synergistic interactions at the interface of nanoparticles (bare colloidal silica) and surfactant (caprylamidopropyl betaine) led to the generation of viscous and stable CO_2-in-water (C/W) foams with fine texture at 19.4 MPa and 50°C. Interestingly, neither species generated C/W foams alone. The surfactant became cationic in the presence of CO_2 and adsorbed on the hydrophilic silica nanoparticle surfaces resulting in an increase in the carbon dioxide/water/nanoparticle contact angle. The surfactant also adsorbed at the CO_2–water interface, reducing interfacial tension to allow formation of finer bubbles. The foams were generated in a beadpack and characterized by apparent viscosity measurements both in the beadpack and in a capillary tube viscometer. In addition, the macroscopic foam stability was observed visually. The foam texture and viscosity were tunable by controlling the aqueous phase composition. Foam stability is discussed in terms of lamella drainage, disjoining pressure, interfacial viscosity, and hole formation. © 2013 American Institute of Chemical Engineers *AIChE J*, 59: 3490-3501, 2013
Keywords: carbon dioxide, nanoparticle, surfactant, foam, viscosity

Introduction

Carbon dioxide has been used for decades for miscible displacement of oil in tertiary enhanced oil recovery (EOR).[1–4] However, CO_2, as a consequence of its low density (~0.05 to 0.5 g/mL) and low viscosity (~0.01 cP), often rises too high in the reservoir (gravity override), or fingers unevenly resulting in poor sweep efficiency.[5,6] The apparent viscosity of CO_2 in porous media may be increased by a factor of 10 to 100+ by forming foams with surfactants that stabilize the aqueous lamellae separating CO_2 bubbles.[6] Traditionally, surfactants have been used to generate emulsions and foams of CO_2 and water by designing the proper hydrophilic/CO_2-philic balance (HCB) of the surfactant, analogous to the hydrophilic/lipophilic balance (HLB).[7]

The HCB influences the interfacial properties of an amphiphile, including the preferred curvature of the CO_2–water interface and the efficiency of the surfactant for lowering the interfacial tension.[8] The HCB has been defined as

$$1/\mathrm{HCB} = \frac{A_{AC} - A_{AA} - A_{CC}}{A_{AW} - A_{AA} - A_{WW}} \quad (1)$$

where $A_{\alpha\beta}$ indicates the interaction pair potential between α and β with A = amphiphile, $C = CO_2$, and W = water.[7,9] For surfactants, the tails contribute primarily to A_{AC} and the head primarily to A_{AW}. A significant challenge to surfactant design for CO_2–water systems is that the low polarizability/volume of CO_2 often results in weak solvation of the surfactant tails resulting in a very high HCB.[7] Here, the surfactant may favor water to such an extent that it adsorbs only weakly at the CO_2–water interface, at a level insufficient for foam formation and stabilization.

The presence of surfactant at the interface may limit foam destabilization via multiple mechanisms, including drainage of lamellae, coalescence, and Ostwald ripening.[10] Surfactants with low HCBs have been used to stabilize water-in-CO_2 (W/C) microemulsions[11–13] and emulsions,[14,15] while surfactants with high HCBs stabilize CO_2-in-water (C/W) emulsions[16,17] and foams.[10] Several studies have focused on nonionic surfactants for C/W emulsions and foams,[10,16,18,19] especially surfactants with "stubby" branched tails to aid in solubilization by CO_2. Various other classes of surfactants have also been investigated for C/W emulsions and foams, including poly(vinyl acetate) surfactants,[18,19] ethoxylated sulfonates,[20,21] sulfobetaines,[20,22] and amines.

Recently, silica nanoparticles have been used to stabilize emulsions and foams with W/C[23] and C/W[9,23–25] curvatures.

Additional Supporting Information may be found in the online version of this article.

Correspondence concerning this article should be addressed to K. P. Johnston at kpj@che.utexas.edu.

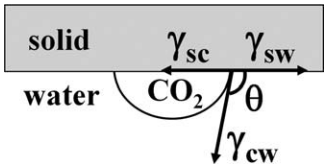

Figure 1. Schematic illustrating the CO_2/water/solid contact angle.

γ_{CW}, γ_{SC}, and γ_{SW} represent the CO_2/water, solid/CO_2, and solid/water interfacial tensions, respectively.

An advantage of nanoparticles for stabilization of CO_2 foams is that they may irreversibly adsorb at CO_2–water interfaces, potentially providing longer term stability than traditional surfactants which dynamically adsorb and desorb at the interface.[26] Nanoparticles can be produced from chemically stable, abundant, low cost, and environmentally benign materials such as silica and clay.[27] Changes in the magnitude of A_{AC} with respect to A_{AW} indicate changes in the wettability of the nanoparticle surface by CO_2 and water. The macroscopic manifestation of the relative interactions between the nanoparticles' surface, CO_2, and water is the contact angle (θ), depicted in Figure 1. The contact angle is generally considered a key parameter for explaining particle behavior at interfaces.[28] However, it is typically only measured for flat surfaces such as silica wafers, rather than for nanoparticles at interfaces.[29–31]

Generally, bare silica nanoparticles are too hydrophilic to stabilize C/W foams,[9] but surface modification by formation of covalent bonds has been used to lower the HCB. Silica nanoparticle surfaces have been modified with CO_2-philic fluorinated ligands for W/C emulsions,[23] hydrophobic dichlorodimethylsilane (DCDMS) for C/W emulsions[25] and foams,[9] and amphiphilic poly(ethylene glycol) (PEG) for C/W foams.[8,24] While providing permanent attachment to the nanoparticle surface, the covalently modified particles often do not lower interfacial tension significantly at oil–water[32] or CO_2–water interfaces.

In situ surface activation of silica nanoparticles by adsorption of surfactant has been demonstrated as a facile route for formation of O/W emulsions[33–36] and A/W foams.[37] This method does not require covalent grafting[37] and also offers the opportunity for free surfactant to adsorb by itself at the oil–water interface to lower interfacial tension (γ). [37,38] Additionally, mixed nanoparticle and surfactant amphiphiles can provide novel interfacial phenomena including double phase inversions based on surfactant concentration[29] and synergistic emulsion formation.[33] Although amine surfactants may be used for *in situ* surface activation of silica nanoparticles, they often cause flocculation of the particles even at low concentrations of surfactant.[33,39] Recently, carboxybetaines have been used for wettability alteration of kaolinite clay particles via electrostatic interaction with negatively charge sites on the clay.[40] Partyka et al.[41] found that carboxybetaines tend to adsorb on silica roughly an order of magnitude lower than protonated amine surfactants of the same tail length at pH 7.5, but their adsorption at lower pH was not investigated. Lower adsorption on silica may be beneficial as higher surfactant concentrations may be used without causing nanoparticle flocculation. Additionally, carboxybetaines are known to have high salinity tolerance and, thus, are of interest for EOR applications.[42–44]

The objectives of this study were to generate viscous and stable C/W foams with fine texture with a mixture of silica nanoparticles and a surfactant and to explain the behavior in terms of interfacial properties. To our knowledge, previous studies have examined either a surfactant or nanoparticle, but not both together. The foam formation is shown to be aided by interfacial tension (γ) reduction from the surfactant, whereas the foam stability may be expected to be augmented by adsorption of nanoparticles at the CO_2–water interface. We utilize a zwitterionic carboxybetaine surfactant caprylamidopropyl betaine (CAPB) that becomes cationic upon protonation in the presence of CO_2. Interestingly, neither the surfactant nor the nanoparticles alone stabilized foam. C/W foams were generated in a beadpack and characterized by the apparent viscosity measurements both in the beadpack and in a capillary tube viscometer, as well as the macroscopic foam stability. The mechanism for the form formation and stability is explained qualitatively in terms of γ and carbon dioxide/water/silica contact angle (θ). To more fully characterize the binary amphiphile, *in situ* surface activation of the nanoparticles with the surfactant was characterized in aqueous solution in terms of dynamic light scattering (DLS) and zeta potential measurements. A key challenge was to design a system whereby the surfactant did not cause the nanoparticles to flocculate. The factors that may have contributed to foam stabilization by the nanoparticle/surfactant composite amphiphiles include lack of excessive amphiphile precipitation at the CO_2–water interface, slow lamella drainage, sufficient disjoining pressure, high interfacial viscosity, and resistance to hole formation. The ability to form stable C/W foams with enhanced stabilities with the combination of nanoparticles and surfactant has the potential to aid advancement of CO_2 EOR.

Materials

Bare colloidal silica nanoparticles (NexSil 20, Nyacol Nano Technologies) were purchased as a 40% aqueous dispersion. CAPB was a gift from Rhodia (Mackam OAB, batch UP1K17X18). As per the certificate of analysis provided by the manufacturer, the solution was 37.6% solids including 6.5% NaCl. The NaCl is a byproduct of the betaine synthesis.[45] As additional impurities are unknown, a concentration of 30% CAPB was assumed for calculations in this study, based on the typical CAPB concentration per the manufacturer.

HCl (1N solution, Fisher Scientific), NaOH (1N solution, Fisher Scientific), NaCl (ACS Grade, Fisher Scientific), HNO_3 (ACS Plus Grade, Fisher Scientific), $NaHCO_3$ (ACS Grade, Fisher Scientific), dodecane (99%, Acros Organics), and CO_2 (research-grade, Matheson) were used as received. Deionized (DI) water (Nanopure II, Barnstead, Dubuque, IA) was used for all experiments.

Methods

Preparation and characterization of aqueous dispersions

Dispersions of nanoparticles with surfactant and/or NaCl in water were prepared by adding dilute nanoparticle dispersions to dilute solutions of CAPB, followed by a solution of NaCl in DI water. All nanoparticle, surfactant, and NaCl concentrations are given as % w/v in the aqueous phase. The NaCl concentrations given in this study are based on the added NaCl to the nanoparticle dispersions and surfactant

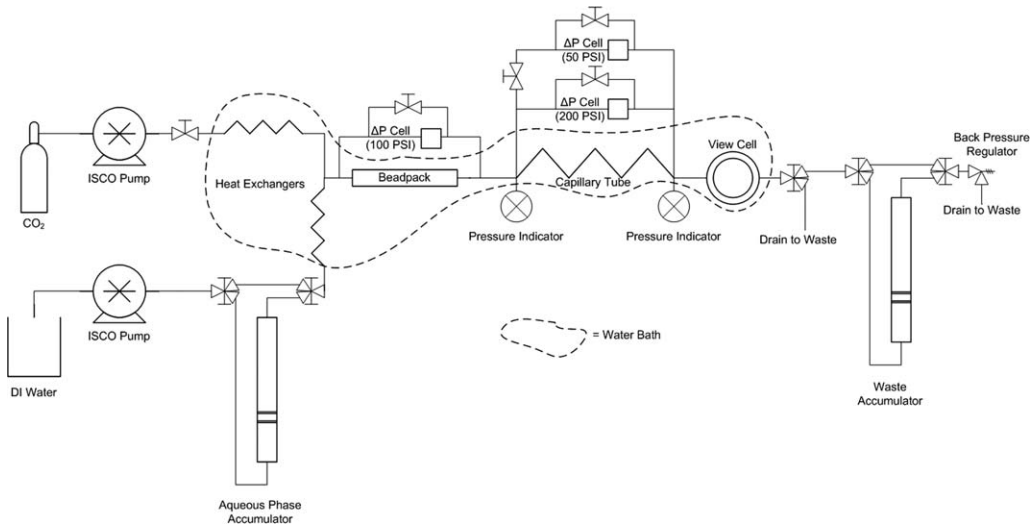

Figure 2. Diagram of apparatus for C/W foam generation, measurement of viscosity and long-term foam stability.

solutions. The NaCl from the stock CAPB solution added an additional 0.002% to 0.1% NaCl for CAPB concentrations of 0.01 to 0.5%, respectively. The additional NaCl was considered insignificant as the nanoparticle/surfactant mixed system behavior was a very weak function of NaCl concentration up to 3% NaCl added to the solution. The nanoparticle and surfactant mixtures were ~pH 8 before any acid or base was added. Where specified, pH was adjusted to 4, 6, or 8 (within ±0.05 pH units) by adding 1N HCl or NaOH solution while stirring and monitoring the pH with a pH meter (Oakton pH 11 series with Oakton WD-35801-00 probe, Oakton Instruments). Dispersions of 0.1% colloidal silica with 0 to 0.5% CAPB were characterized at room temperature (22 ± 1°C) with a Brookhaven ZetaPALS instrument to determine the zeta potential and the hydrodynamic diameter of the particles. The Smoluchowski equation was used to convert the measured mobility to zeta potential and the CONTIN model was used to fit the DLS data.

Determination of surfactant isoelectric point

Titration was used to determine the isoelectric point (pI) of the surfactant where 100 mL of 1% CAPB solution was first adjusted to pH 10.09 with 2.4 N NaOH solution and then 5–50 μL aliquots of 1N HCl solution were added while stirring the surfactant solution. The pH of the surfactant solution was measured with a pH meter (Oakton pH 11 series with Oakton WD-35801-00 probe, Oakton Instruments) and recorded after each aliquot of HCl solution was added.

Interfacial tension and contact angle measurements

Axisymmetric drop shape analysis of a captive bubble was used to determine the CO_2–water interfacial tension (γ) and the contact angle (θ) between CO_2/water/silica wafer. The apparatus and techniques were adapted from previous studies of interfacial tension[46] and contact angle.[31] The high-pressure cell that held the stage was pressurized with CO_2 to 6.65 MPa (absolute) and held at room temperature (22 ± 1°C). The solution was stirred for 30 min with excess CO_2 present to ensure that the aqueous phase was saturated with CO_2 before measurements were taken. The CO_2 bubble profile shape when captured on the stage was analyzed according to the Laplace equation to calculate γ and θ made with the stage. The average and standard deviation of the calculated interfacial tension or contact angle for four bubbles were recorded, where 10 measurements were taken of each bubble every 5 s. For interfacial tension measurements, the stage was cut from a polished quartz wafer (item number SOX101005S2 from MTI Corp.). For contact angle measurements, the stage was cut from a silica-coated silicon wafer. To produce the silica coating on the silicon wafer (mirror-polished Si, Wafer World), it was cleaned with DI water and placed in 15.8 N HNO_3 solution overnight.[33] The resulting silica-coated wafer was then neutralized with $NaHCO_3$, washed with DI and ethanol, and dried prior to use.

C/W foam formation, apparent viscosity measurement, and stability determination

The C/W foams were formed and characterized in an apparatus described elsewhere.[9] A diagram of the apparatus used to generate C/W foams is shown in Figure 2. Nanoparticle dispersions were prepared as described above, without adjusting the pH prior to use. All experiments were done at 19.4 MPa (absolute) and 50°C, using a total flow rate of 1.5 mL/min and a CO_2:water phase ratio of 3:1 by volume. The system pressure was maintained within 0.2 MPa for all experiments. The apparent viscosity of the foam in the beadpack (0.38 cm ID × 11.3 cm long, filled with 180 μm spherical glass beads, porosity of 0.34, pore volume of 0.436 mL, and permeability of 22.5 darcy) was calculated from the pressure drop using Darcy's Law, treating the foam as a single phase.[1] At a flow rate of 1.5 mL/min, the shear rate in the beadpack is 1130 s^{-1}, the superficial velocity is 0.220 cm/s, and the residence time is 17.4 s. The beadpack shear rate and superficial velocity used in this study may be found in field applications near an injection well where most foam generation is expected.[6] The apparent viscosity of the foam in the capillary tube (0.0762 cm ID × 195 cm long, volume of 0.889 mL, and permeability of ~19,000 darcy) was calculated from the pressure drop across the capillary tube using the Hagen–Poiseuille equation. At a flow rate of 1.5 mL/min, the shear rate at the wall of the capillary tube is 576 s^{-1}, the superficial velocity is 5.482 cm/s, and the residence time is 35.6 s. Per manufacturer's information, the accuracy of the differential pressure reading is ±0.25% of full scale,

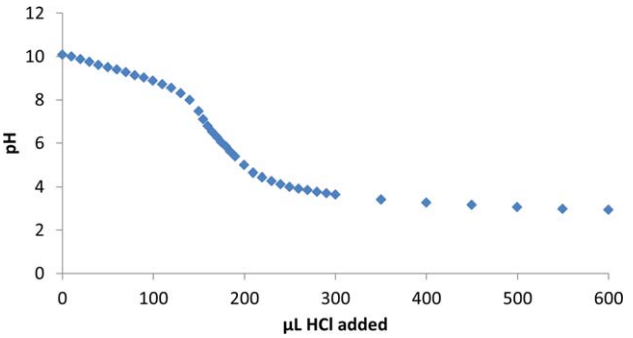

Figure 3. Titration curve of 100 mL 1% w/v CAPB with 1 N HCl.

The inflection point at pH ~ 6.4 indicates the isoelectric point (pI) of the surfactant. [Color figure can be viewed in the online issue, which is available at wileyonlinelibrary.com]

which is equivalent to ±0.15 cP in the capillary and ±0.31 cP in the beadpack.

O/W emulsion formation, stability, and microstructure determination

To generate O/W emulsions, 1.5 mL of nanoparticle dispersion and 1.5mL of dodecane were loaded into a 1 dram vial (capacity of 3.7 mL) and sonicated for 1 min with a Branson Sonifier (VWR Scientific, model 250) equipped with a microtip. The microtip was held just above the oil–water interface to avoid entraining air during O/W emulsion formation. Digital photographs were taken of the vials to record macroscopic emulsion behavior. Microstructure was recorded with optical micrographs of the emulsions. The micrographs were taken of 20 µL of O/W emulsion removed from the center of the emulsion phase and placed on a slide with a glass cover slip. Droplet sizes were measured using ImageJ software, using a calibration slide as a standard.

Results

Isoelectric point determination

The CAPB surfactant was titrated with HCl to find the isoelectric point (pI) in DI water. Figure 3 shows the pH of a 1% CAPB sample as a function of added HCl solution, where the pI is indicated by the inflection point at pH ~ 6.4. For the experiments in this study where CO_2 and water are present, the pH will be well below this point and the surfactant will be positively charged (Scheme 1).

DLS and zeta potential measurements

DLS was used to determine the hydrodynamic diameter of the silica particles as a function of CAPB concentration at pH 4 and 6 (Figure 4a). The results show consistent particle hydrodynamic diameters of ~28 nm at CAPB concentrations up to 0.25%, indicating that no detectable particle flocculation occurred after 40 h of aging.

Figure 4b shows the zeta potential of silica nanoparticles (0.1%) at pH values of 4, 6, and 8 as a function of CAPB concentration. The zeta potential of the nanoparticles was strongly negative without surfactant as expected for silica. At pH 4, where the surfactant is cationic, the zeta potential increased much more strongly than at pH 6 where it was zwitterionic. At pH 8, where it was mildly anionic, the number of negative charges added by the surfactant appeared to be lower than the number of negative charges lost from the silica. With the lower local dielectric constant from the adsorbed surfactant and increase in the number of silanol groups with adsorbed hydrophobe from the surfactant tail, the number of dissociated silanol groups appears to have decreased. At pH 4 with 0.5% CAPB, the nanoparticle dispersion became opaque immediately after preparation and showed significant settling in 1–2 min as the electrostatic repulsion became small.

Captive-bubble interfacial tension and contact angle measurements

The results of the CO_2 captive bubble γ and θ measurements are summarized in Table 1. The high-pressure cell was held at room temperature (22 ± 1°C) and 6.65 MPa. A temperature of 22°C was assumed for fitting the bubble profile. At these conditions, CO_2 is a liquid and has a density of 0.772 g/mL. As solvation of surfactant tails by CO_2 is known to be a strong function of density,[7] these conditions were chosen to give a similar CO_2 density to the target foam formation conditions (50°C and 19.4 MPa), where the CO_2 density is 0.776 g/mL. A CAPB concentration of 0.25% in the water phase decreased the CO_2–water interfacial tension by 11.9 mN/m and caused the CO_2/water/silica θ to increase by 11.5°. An attempt was made to determine the solubility of CAPB in CO_2 at a fixed CAPB concentration of 0.15% w/w. Even at 34.6 MPa and 22°C, it was not soluble. Thus, in the captive bubble and θ measurements the concentration of surfactant in the CO_2 phase may be assumed to be small, such that the surfactant concentration in the water phase remained essentially constant.

C/W foam texture and viscosity

C/W foams were generated at 50°C and 19.4 MPa with a CO_2:water phase ratio of 3:1 by volume. CO_2 is a supercritical fluid at these conditions with a density of 0.776 g/mL, very similar to the density used for γ and θ measurements. Representative examples of C/W foam texture are given in Figure 5, showing a very fine foam (Figure 5a), an intermediate texture (Figure 5b), and a very coarse foam (Figure 5c). The example fine texture foam was generated with 1% silica nanoparticles and 0.05% CAPB with 1% NaCl in solution. The example intermediate texture foam was generated with a lower silica nanoparticle concentration of 0.1%, resulting in large CO_2 bubbles. The example coarse foam was also generated with 0.1% nanoparticles, but with no salt present. These examples demonstrate that the texture of the foam may be tuned by adjusting the aqueous phase composition.

The apparent viscosity of the CO_2 and aqueous phase mixture in the beadpack and capillary tube are summarized in Figures 6 and 7, respectively. For all of these foams, the highest viscosity foams (> 10 cP in capillary and > 50 cP in beadpack) were very white with fine texture as shown in Figure 5a. Foams with intermediate viscosities (5–10 cP in capillary and 25–50 cP in beadpack) tended to have

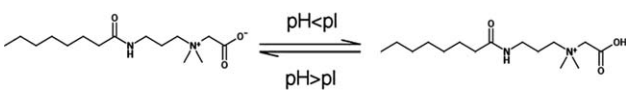

Scheme 1. CAPB reversibly switches between a zwitterion above the pI and a cation below the pI.

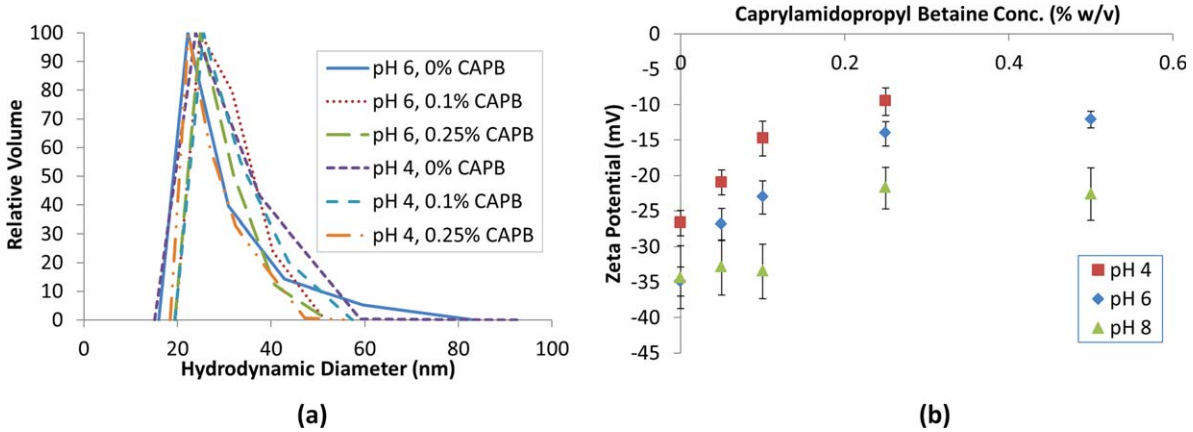

Figure 4. (a) Size distributions of 0.1% w/v bare colloidal silica measured by DLS at pH 4 and 6 with 0%, 0.1%, and 0.25% CAPB after aging for 40 h.

The average hydrodynamic diameter for each run was 28 ± 2 nm. (b) Zeta potential of 0.1% w/v bare colloidal silica at pH 4, 6, and 8 as a function of CAPB concentration. [Color figure can be viewed in the online issue, which is available at wileyonlinelibrary.com]

intermediate texture as shown in Figure 5b. Low viscosity foams (2–5 cP in capillary and 10–25 cP in beadpack) had very coarse textures as shown in Figure 5c. When the mixture viscosity was less than ~2 cP in the capillary and less than ~10 cP in beadpack, at most only single lamellae were visible in the view cell indicating no foam was observed.

Figures 6 and 7 show the apparent viscosity as a function of silica nanoparticle concentration while holding the CAPB concentration fixed at 0.05% (Figures 6a and 7a), and as a function of CAPB concentration while holding the nanoparticle concentration fixed at 1% (Figures 6b and 7b). Salinities of 0%, 1%, and 3% NaCl are shown for both concentration variation methods. When the CAPB concentration was held constant, the salinity did not affect the apparent viscosity. A weak increase in viscosity with increased salinity was observed when the nanoparticle concentration was held constant (Figures 6b and 7b). In both the beadpack and the capillary, foam was not formed with either surfactant or nanoparticles. However, in each case the foam viscosity increased with increasing nanoparticle concentration or CAPB concentration, while holding the other species constant. The values of viscosity reached 36 cP in the capillary, which is quite large for a surfactant concentration of only 0.05%. The rate of increase of the viscosity as a function of nanoparticle concentration between 1.5% and 3% slowed significantly in both the beadpack (Figure 6a) and capillary tube (Figure 7a). The rate of increase as a function of CAPB concentration between 0.1% and 0.5% slowed significantly in both the beadpack and the capillary. Interestingly, the apparent viscosity of the foam was higher in the beadpack than in the capillary for all but the lowest viscosity experiments (Supporting Information Figure S1). The nanoparticle dispersions did not visibly flocculate between creation and the end of the foam experiment (2–12 h) at the conditions tested in this study. Periodically, the beadpack permeability was tested with DI water to verify that the beadpack properties had not measurably changed due to filtration or irreversible adsorption of nanoparticle and surfactant aggregates. No decrease in permeability from the initial value of 22.5 darcy was noted throughout the experiments, indicating the nanoparticles did not appreciably plug the pore throats.

C/W foam stability

After foam formation and viscosity characterization, two foams were held in the view cell for 20 h to observe their long-term stability. Foam generated with 1.5% bare colloidal silica and 0.05% CAPB (0% NaCl) is shown in Figures 8a, b, immediately after the flow experiment was stopped and after 20 h, respectively. The initial viscosity of the foam was 70 cP in the beadpack and 36 cP in the capillary. No foam resolution (by height) was observed, but the foam did become slightly less opaque white. Foam generated with 1% bare colloidal silica and 0.1% CAPB at a salinity of 3% NaCl is shown in Figures 8c, d, immediately after the flow experiment was stopped and after 20 h, respectively. The initial viscosity of the foam was 71 cP in the beadpack and 34 cP in the capillary. The foam became noticeably less opaque white in the upper 20% of the cell, but remains very opaque white throughout the rest of the volume. Stability observations lasting weeks or months may also be of interest for EOR applications, but were outside the scope of this study.

Effect of pH on interfacial properties

To investigate the effect of pH on the interfacial properties of the nanoparticle/surfactant mixed system, dodecane-in-water emulsions (1:1 dodecane:aqueous phase, by volume) were generated at pH values of 4, 6, and 8. The aqueous phases chosen were 1% bare colloidal silica with 0.05% CAPB, and 1% bare colloidal silica with 0.05% CAPB (concentrations given in aqueous phase). The emulsified volume of dodecane and emulsion macroscopic texture are shown in Figure 9 after 1 h of aging. In the nanoparticle-only emulsions (left column), the amount of dodecane emulsified

Table 1. Effect of CAPB on γ and θ at 22°C and 6.65 MPa ($\rho_{CO_2} = 0.772$)

Aqueous Phase	$\gamma \pm$ Std. Dev. (mN/m)[a]	$\theta \pm$ Std. Dev. (°)[b]
DI water	28.3 ± 1.0	28.1 ± 1.3
0.25% w/v CAPB	16.4 ± 1.4	39.6 ± 1.6

[a]Measured using polished quartz wafer.
[b]Measured using silica-coated wafer.

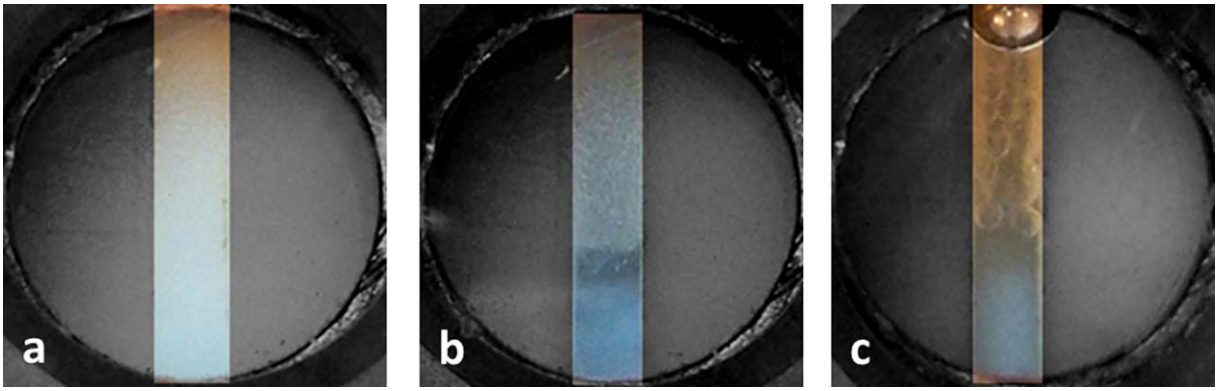

Figure 5. Representative examples of C/W foam in the view cell at 50°C, 19.4 MPa with (a) fine texture, (b) intermediate texture, and (c) coarse texture.

Foam is visible in the center of the window in the vertical channel between Teflon spacers. The Teflon spacers have been darkened with photo editing software to highlight the channel. Dark regions in the channel indicate absence of foam. Window diameter is 1.4 cm and visual path length is 0.8 cm. [Color figure can be viewed in the online issue, which is available at wileyonlinelibrary.com]

decreased from pH 4 to pH 6 to pH 8. Also, the emulsions were not opaque white, which indicates that they are likely composed of very large or very disperse droplets. In the surfactant-only emulsions (center column), no significant fraction of dodecane was emulsified at any pH tested. In the mixed surfactant/nanoparticle emulsions (right column), no excess dodecane was visible after emulsification at all pH conditions tested. The amount of excess water phase increased from pH 4 to pH 6 to pH 8, and the emulsion also looked less bright white at pH 8, likely indicating larger or more disperse droplets.

To further investigate the microstructure of the surfactant and nanoparticle stabilized emulsions, micrographs were taken of emulsified oil droplets after 1 day (Figure 10) and 14 days (not shown). The average droplet sizes increased slightly from pH 4 to 6 and significantly increased at pH 8. The oil droplet size distribution is given in Supporting Information Figure S2 at pH 4, 6, and 8 at 1 day and 14 days. The average droplet sizes remained constant after 14 days, as did the droplet-size distributions (Supporting Information Figure S2).

Discussion

Nanoparticle and surfactant effect on CO_2–water γ

Surfactants with the proper HCB can adsorb at the CO_2–water interface to reduce the interfacial tension. The surface pressure of the surfactant, Π_s, defined by $\gamma_o - \gamma$, where γ_o is the interfacial tension between CO_2 and water without surfactant, may be used to define the surfactant efficiency. In the present study, 0.25% (w/v) CAPB had a moderate surface pressure of 11.9 mN/m at 22°C and 6.65 MPa (CO_2 density of 0.772 g/mL). At CO_2 densities of 0.75–0.78 g/mL, Adkins et al.[8] and Chen et al.[46] found Π_s in the range of 18 to 26 mN/m for several ethoxylated nonionic surfactants at concentrations of only 0.01%. The ethoxylated nonionic surfactants had molecular weights of 3× to 4× that of CAPB, which may contribute to greater Π_s values and surfactant efficiencies. The poor efficiency of CAPB (low Π_s) may be a consequence of a very high HCB, reflecting limited solubilization by CO_2 of the hydrophobic tail compared to strong solubilization by water of the quaternary amine in the head group. The head group interactions include charge–dipole interactions as well as hydrogen bonding with the

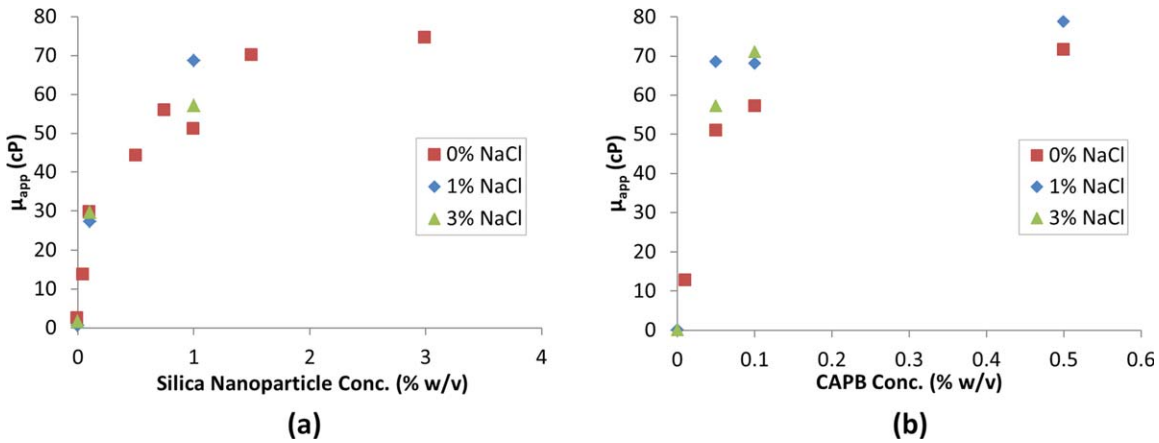

Figure 6. Particle-surfactant mixture stabilized C/W foam viscosity measured in the beadpack with 0%, 1%, and 3% w/v NaCl at 50°C, 19.4 MPa.

Viscosity is shown as a function of (a) silica nanoparticle concentration with fixed 0.05% CAPB concentration and (b) CAPB concentration with fixed 1% silica nanoparticle concentration. [Color figure can be viewed in the online issue, which is available at wileyonlinelibrary.com.]

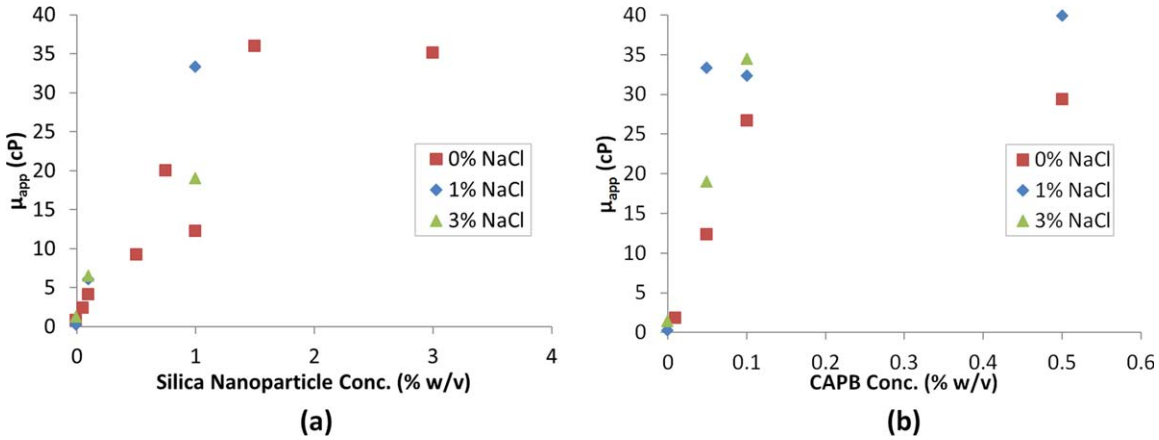

Figure 7. Particle-surfactant mixture stabilized C/W foam viscosity measured in the capillary tube with 0%, 1%, and 3% w/v NaCl at 50°C, 19.4 MPa.

Viscosity is shown as a function of (a) silica nanoparticle concentration with fixed 0.05% CAPB concentration and (b) CAPB concentration with fixed 1% silica nanoparticle concentration. [Color figure can be viewed in the online issue, which is available at wileyonlinelibrary.com]

carboxylic acid. The amide group in the surfactant "tail" also has a hydrogen bond acceptor (—C═O—) and donor (—NH—),[47] and thus would also likely prefer to interact with water than CO_2, contributing further to the high HCB. The efficiency of carboxybetaine surfactants at lowering interfacial tension is expected to be a function of pH, as

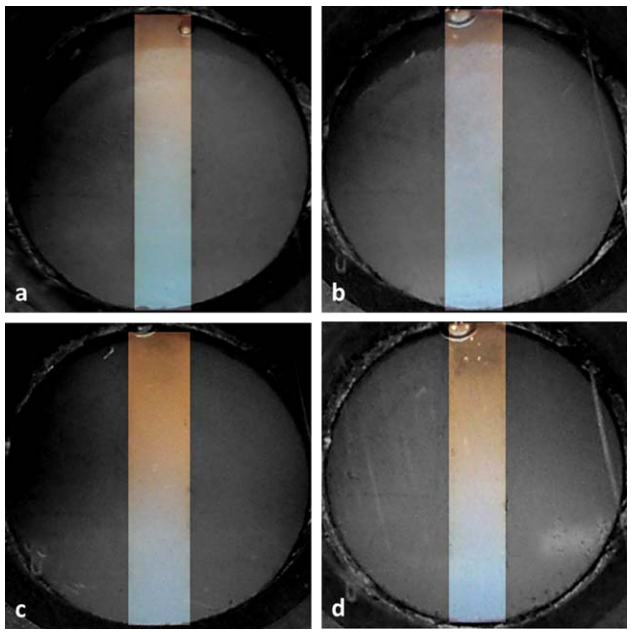

Figure 8. C/W foam stability in view cell at 50°C, 19.4 MPa.

(a) and (b) are 1.5% silica nanoparticles + 0.05% CAPB, $t = 0$ and 20 h, respectively. (c) and (d) are 1% silica nanoparticles + 0.1% CAPB + 3% NaCl, $t = 0$ and 20 h, respectively. Foam is visible in the center of the window in the vertical channel between Teflon spacers. The Teflon spacers have been darkened with photo editing software to highlight the channel. Dark regions in the channel indicate absence of foam. Window diameter is 1.4 cm and visual path length is 0.8 cm. [Color figure can be viewed in the online issue, which is available at wileyonlinelibrary.com]

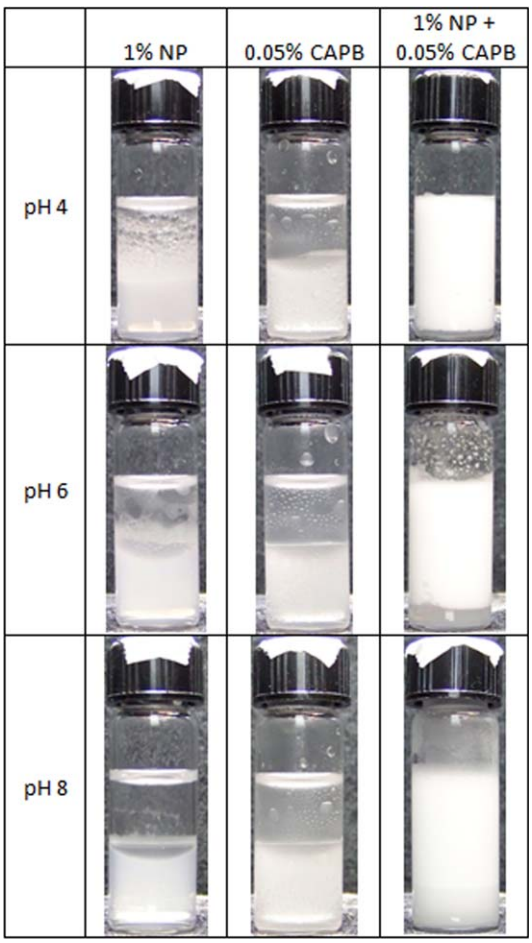

Figure 9. O/W emulsions prepared with 1:1 dodecane:-water (by volume) stabilized at pH 4, 6, and 8 with 1% silica nanoparticles (NP), 0.05% CAPB, and 1% NP + 0.05% CAPB.

Photographs taken 1 h after emulsion formation. The outside diameter of the vials is 1.47 cm. [Color figure can be viewed in the online issue, which is available at wileyonlinelibrary.com]

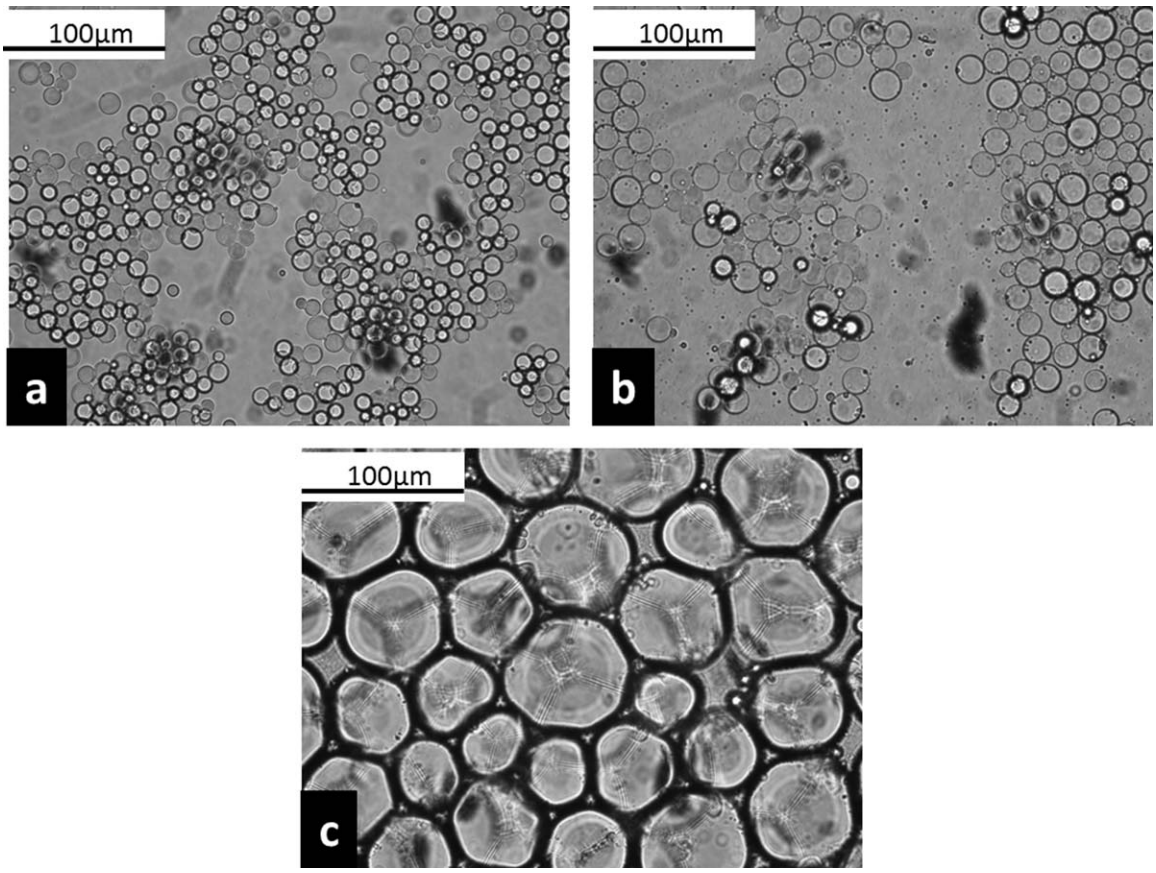

Figure 10. Optical micrographs of emulsions stabilized with 1% silica nanoparticles (NP) + 0.05% CAPB at (a) pH 4; (b) pH 6; and (c) pH 8.

Micrographs taken 1 day after emulsion formation.

protonation of the carboxylic acid group in the surfactant head group makes the surfactant cationic[48] and, thus, more hydrophilic. In a CO_2–water saturated system, the pH would naturally fall below the pI of the surfactant for CO_2/water systems and, thus, would always be in the higher HCB cationic form. In the presence of an excess CO_2 high pressure supercritical fluid phase, the CO_2 is a strong buffer and it becomes difficult to raise the pH above about 6 even with strong base.[49]

When silica nanoparticles and betaine surfactant are used together in the aqueous phase, intermediate γ lowering is expected compared to a system without nanoparticles present. Bare silica nanoparticles alone are not expected to lower interfacial tension based on previous studies at the oil/water interface (Vignati), although this phenomena is not fully understood. Nanoparticles coated with amphiphilic polymers may decrease γ, which has been observed in oil–water systems with iron oxide nanoparticles coated with copolymers of poly(acrylic acid) and poly(butyl acrylate)[50] and silica nanoparticles grafted with poly(styrene sulfonate)[51] and poly(2-(dimethylamino)ethyl methacrylate).[52] The polymers in these studies had molecular weights between 12 kDa and 30 kDa, and can interact with a large interfacial area to provide γ reduction.

In the current work, surfactant that is not adsorbed to the silica nanoparticles would be free to adsorb at the CO_2–water interface to lower the interfacial tension. The relative affinity of surfactant for adsorption at the CO_2–water and silica–water interfaces would likely be a function of pH as well, where weak adsorption on the nanoparticles would leave more surfactant free to adsorb at the CO_2–water interface to lower γ.

Surfactant effect on contact angle

The contact angle between a nanoparticle surface (P) with CO_2 and water is controlled by the interfacial tensions between the three phases, as described by Young's equation

$$\cos\theta = \frac{\gamma_{PC} - \gamma_{PW}}{\gamma_{CW}} \tag{2}$$

where the nomenclature is shown in Figure 1. Silica surfaces contain deprotonated silanol groups (SiO^-) above pH ~2. The surfaces are expected to have a high γ_{PC} and a low γ_{PW} because of the weak and strong solvency for charged species by CO_2 and water, respectively.[31] If surfactant adsorbs on the silica surface such that the head group interacts with the negatively charged surface,[41,53] the effective surface charge will be reduced and the surfactant hydrophobic tail will add hydrophobicity.

As there is great difficulty in accurately determining nanoparticle contact angles at fluid–fluid interfaces,[53,54] this study used a flat silica surface as a model for the silica nanoparticle surfaces, following the method reported by Binks et al.[33,55] The experimentally observed increase in θ between CO_2/water/silica wafer with added surfactant (decrease in $\cos\theta$) indicates that the decrease in the numerator was larger than that in γ_{cw}. The decrease in $\gamma_{PC} - \gamma_{PW}$ with surfactant may be explained from the hydrophilicity. The adsorbed

surfactant decreases the hydrophilicity (raises γ_{PW}). This change may be expected to reduce γ_{PC} and raise γ_{PW} as observed, but the individual changes in γ_{PC} and γ_{PW} are unknown.[56]

The observed asymptotic trend in increasing zeta potential (Figure 4b) suggests that a surfactant bilayer or hemimicelle layer was not formed on the nanoparticle surface under the conditions investigated.[29] If so, we would have expected the zeta potential to become positive due to the added cationic surfactant head groups. The observed increase in θ on a flat silica surface and the absence of bilayer or hemimicelle formation suggest that the CO_2/water/nanoparticle surface θ increases monotonically with adsorbed surfactant under the conditions investigated.

Foam formation, texture, and viscosity

To form a CO_2 bubble or droplet, the external (shear) stress applied to the interface must exceed the Laplace pressure (P_c), where $P_c = 2\gamma/R$. The balance between the applied stress and P_c can be described by the Weber number

$$\mathrm{We} = \frac{G\mu_s R}{\gamma} \tag{3}$$

where G is the shear stress (du/dz), μ_s is the continuous phase shear viscosity, and R is the bubble radius.[57] Above a critical value of We, the shear breaks up the droplets into smaller ones.[57] The low γ of CO_2–water binary systems (20–30 mN/m) contributes to a larger We and may aid in the formation of smaller bubbles (fine texture foams) than for oil/water emulsions. The presence of nanoparticles and surfactant may further increase We by increasing μ_s and decreasing γ, respectively. Together, nanoparticle and surfactant mixed systems were shown to favor smaller bubbles (finer foams) than either nanoparticles or surfactant alone in Figure 5c. Once formed, nanoparticles and surfactant can adsorb on the bubble surfaces to sufficiently stabilize them for viscosity measurement and texture observation (~1 min).

There was a strong correlation between foam texture and viscosity in the present study, which is expected based on the work by several investigators.[58–60] The formation of foam increases the apparent viscosity of a dispersed gas phase because of slugs of liquid between bubbles, resistance to deformation by the bubbles, and surface tension gradients across bubbles.[59] Finer foams have more lamellae and bubbles per unit length than coarser foams, and thus are expected to produce higher viscosities.

Foams tended to show higher viscosities in the beadpack than in the capillary, which may be due to several factors governing the foam rheology. Falls et al.[61] discussed the influence of capillary pressure on the curvature of lamellae in porous media as well as the presence of pore constrictions which can add resistance to lamellae movement through the beadpack. Furthermore, foam formation is expected in the beadpack, where lamellae are continuously created by mechanisms such as leave-behind, snap-off, and lamella division.[6] The shear rate is higher in the beadpack than in the capillary as well, and shear thickening behavior is often seen in foam flows, and is dictated by quality.[62]

The viscosity and texture of the foams were influenced markedly by the presence of both the nanoparticles and the surfactant (Figures 6 and 7). The synergistic behavior of the mixed surfactant and nanoparticle system was evident in that neither the surfactant alone nor the nanoparticles generated foams. Similar synergy has been observed in terms of foam or emulsion formation in A/W[37] or O/W[29,63] systems, respectively. For example, Cui et al.[29] used short fatty acids with cationic $CaCO_3$ nanoparticles to generate toluene-in-water emulsions, whereas the nanoparticles or the shortest fatty acids alone were poor stabilizers. The synergistic emulsion formation was attributed to the *in situ* surface activation of the nanoparticle with adsorbed fatty acids, demonstrated by decreased zeta potential of the positively charged particles and increased θ of air/water/bulk $CaCO_3$ surface. The short fatty acids alone were not expected to significantly lower γ, but fine bubbles were generated due to the high G provided by a homogenizer. In the current study, the surfactant was effective at both *in situ* surface activation of the silica nanoparticles, as shown in the zeta potential, and in lowering γ, allowing for generation of finely textured foams with the low G provided by the sandpack.

We propose that the nanoparticle and surfactant adsorbed together at the CO_2–water interface to allow foams to flow through the beadpack and capillary tube and be observed in the viewcell. A simplified configuration of the adsorbed species at the CO_2–water interface is given in Figure 11a, which has been adapted from other investigators.[29,55] The surfactant may either be free in water, independent of the nanoparticles at the CO_2–water interface or adsorbed on the nanoparticle surface. The model is consistent with the decreased surface charge of the silica nanoparticles due to adsorption of the protonated carboxybetaine surfactant, increased contact angle of the *in situ* surface activated nanoparticles adsorbed at the CO_2–water interface, and decreased γ due to surfactant adsorbed at the CO_2–water interface. The model of the potential positions of the amphiphiles will be utilized below to explain the mechanisms responsible for the stabilization of the CO_2–water interface.

Stabilization mechanisms

Lamella Drainage. In a C/W foam, aqueous lamellae separate CO_2 bubbles and prevent the bubbles from coalescing. The lamellae experience a disjoining pressure (Π_d)[64–66] due to electrostatic, steric, structural, and additional short-range repulsive forces which counteract the van der Waals attraction between the two film surfaces.[10,67] The cationic protonated CAPB and the anionic nanoparticles will contribute electrostatic repulsion to Π_d; however, the opposite charges for the two amphiphiles will cause some cancellation of charge. The nanoparticles may also contribute to Π_d via structural effects that increase the osmotic pressure due to organization of particles in the lamella[66,68,69] and contribute mechanical disjoining forces due to nanoparticle flocs "bridging" the lamellae.[54] The liquid in the lamellae drains due to gravity and capillary forces which reduces lamellae thickness. The contribution due to gravity is ignored in this discussion because of the relatively high density of CO_2 (0.776 g/mL), the small bubble size, and the fact the lamellae are very thin. The drainage due to capillary forces, described by Reynolds for the flow of liquid from between two approaching solid plates, may be expressed as

$$V_{RE} = \frac{-dh_f}{dt} = \left(\frac{{h_f}^3}{3\mu_c {R_{film}}^2}\right)\Delta P_{film} \tag{4}$$

where h_f is the film thickness, R_{film} is the film radius, and $\Delta P_{film} = 2(P_c - \Pi_d(h_f))$.[70] Thus, a decrease in P_c due to a reduction in γ with surfactant and an increased Π_d due to

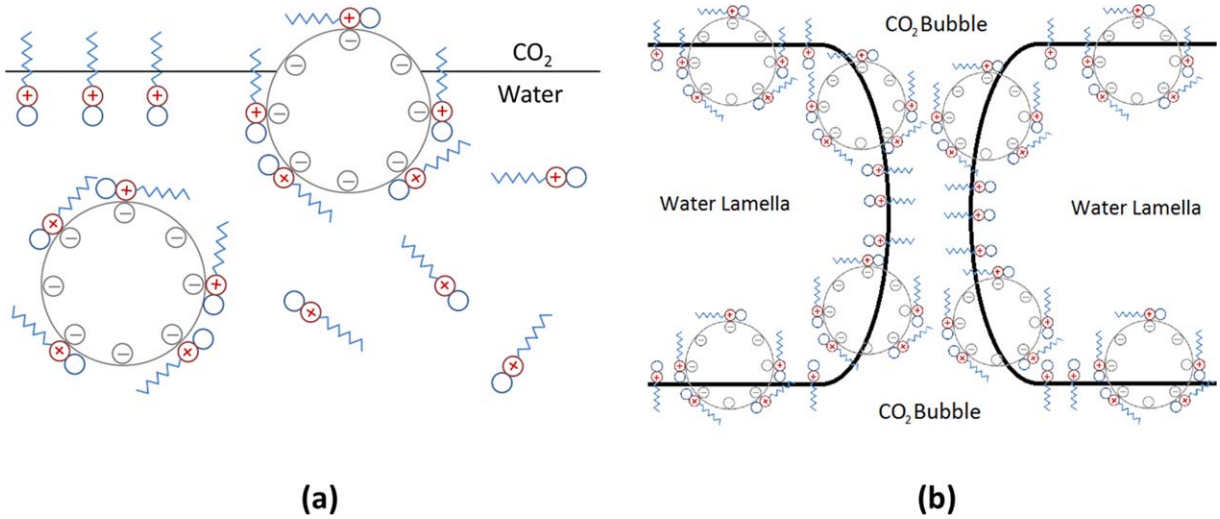

Figure 11. Simplified schematic of silica nanoparticles with protonated carboxybetaine surfactant at (a) a CO_2–water interface; (b) in an aqueous lamella between CO_2 bubbles connected by a CO_2 hole.

[Color figure can be viewed in the online issue, which is available at wileyonlinelibrary.com]

both nanoparticles and surfactant may be expected to slow film drainage. Marangoni stabilization, which increases with gradients in γ,[71] may further provide resistance to flow and contribute to stabilization of lamellae.

In the Reynolds equation (Eq. 4), the viscosity of the aqueous lamella (μ_c) is considered constant, which may be an oversimplification. Adsorbed nanoparticles may increase the interfacial viscosity,[72–75] which may further slow lamella drainage and stabilize foams.[74,76] Murray et al.[74] measured the interfacial viscosity of *n*-tetradecane/water interface and found a synergistic increase when both starch particles and sodium caseinate, an interfacially active protein, were adsorbed at the interface. The increase in interfacial viscosity due to adsorbed nanoparticles may slow diffusion of species near the interface, further contributing to stability. For example, an increase in interfacial viscosity could be beneficial in slowing Ostwald ripening, which can be significant in C/W foam destabilization due to the appreciable solubility of CO_2 in water.

Hole Formation. Foams may be destabilized by coalescence due to hole formation in the aqueous lamellae separating bubbles. Holes appear because of thermal fluctuations that produce spatial and density variations in the film.[77,78] Lamellae drainage acts to thin the aqueous lamellae, which reduces the work required to open a hole and increases the probability of hole formation.[79] If the radius of the hole exceeds a critical value, then the hole will grow and the foam film will rupture. Adkins et al.[10] considered the formation of a CO_2 hole in a C/W/C film stabilized with a surfactant that prefers the aqueous phase. They proposed that the weak solvation of hydrocarbon tails by the CO_2 phase upon the start of hole formation would resist bending of the interface and arrest growth of the hole and prevent coalescence.

The nanoparticles in the present study also prefer the aqueous phase, and are also expected to resist bending of the interface to allow a CO_2 hole to form in lamellae. The adsorption energy, E, for a uniformly coated nanoparticle at a CO_2–water interface is given by

$$E=\pi r^2\gamma(1\pm\cos\theta)^2 \tag{5}$$

where r is the particle radius.[28] A 28 nm diameter particle at a CO_2–water interface with surfactant lowering γ to 17 mN/m would have an $E = 10^3$ to 10^4 kT, depending on θ. This energy would provide essentially irreversible adsorption to the CO_2–water interface and the orientation of the nanoparticle more toward the water side would provide a barrier to resist interface bending to produce a CO_2 channel curved about water on each side of the channel (Figure 11b). Quantitatively, bending of the interface to expose more nanoparticle surface to the CO_2 phase would be unfavorable, as changing θ by even 1° would require an energy of 10^1-10^2 kT. Furthermore, this bending would expose more surfactant tails to CO_2, which is also unfavorable. Thus, we propose that both the nanoparticles and surfactant would tend to resist hole formation via CO_2–water interface bending about water.

Conclusions

Viscous and stable C/W foams with fine texture were generated with a nanoparticle (bare colloidal silica) and surfactant (CAPB) mixture and described in terms of the relevant interfacial phenomena that influence foam texture, viscosity, and stability. The foam formation was aided by interfacial tension (γ) reduction from the surfactant, while the foam stability may be expected to be augmented by adsorption of nanoparticles at the CO_2–water interface. Electrostatic interactions between the cationic portion of the surfactant head group and the negatively charged silica surface facilitated adsorption of surfactant on the silica nanoparticles, reducing the HCB of the nanoparticles. The lower HCB increased adsorption at the CO_2–water interface. The *in situ* surface activation of silica with adsorbed surfactant was characterized in terms of an increased zeta potential of the silica nanoparticles and an increased CO_2/water/silica contact angle. The nanoparticle/surfactant dispersion remained stable as demonstrated by DLS, as surfactant tail–tail interactions were too weak to cause flocculation of the nanoparticles. The adsorption of surfactant at the CO_2–water interface did not lower the interfacial tension enough for foam formation. However, in the presence of the silica nanoparticles textured foams were formed with bubbles too small to be visible (<100 μm diameter with a maximum viscosity of 79 cP in the beadpack and 36 cP in the capillary tube. The surfactant

and nanoparticles also imparted long-term stability to the foam, where no resolution (by height) occurred in 20 h for the most stable foam observed. The stability was favored by various factors including an increase in disjoining pressure and interfacial viscosity, which mitigate lamella drainage and Ostwald ripening, and the unfavorable bending of the interface around the water phase, which resists hole formation.

Acknowledgments

This work was supported by the Department of Energy National Energy Technology Laboratory under Award Number DE-DE0005917, the Center for Frontiers of Subsurface Energy Security, the Gulf of Mexico Research Initiative, and the Robert A. Welch Foundation (F-1319).

Literature Cited

1. Lake L. Enhanced Oil Recovery. Englewood Cliffs, NJ: Prentice Hall, 1989.
2. Heller JP. CO_2 foams in enhanced oil recovery. In: Schramm LL, ed. *Advances in Chemistry Series*. Vol 242 (Foams: Fundamentals and Applications in the Petroleum Industry). Washington, DC: American Chemical Society; 1994:201–234.
3. Orr FM Jr, Heller JP, Taber JJ, Card RJ. Carbon dioxide as solvent for oil recovery. *Chemtech*. 1983;13(8):482–487.
4. Pope GA. The application of fractional flow theory to enhanced oil recovery. *SPE J*. 1980;20(3):191–205.
5. Rossen WR, Gauglitz PA. Percolation theory of creation and mobilization of foams in porous media. *AIChE J*. 1990;36(8):1176–1188.
6. Rossen WR. Foams in enhanced oil recovery. In: Prud'homme RK, Khan SA, editors. Foams: Theory, Measurements, and Applications, Vol. 57. New York: Marcel Dekker, 1996.
7. Johnston KP, Da Rocha SRP. Colloids in supercritical fluids over the last 20 years and future directions. *J Supercrit Fluids*. 2009;47:523–530.
8. Adkins SS, Chen X, Nguyen QP, Sanders AW, Johnston KP. Effect of branching on the interfacial properties of nonionic hydrocarbon surfactants at the air–water and carbon dioxide–water interfaces. *J Colloid Interface Sci*. 2010;346(2):455–463.
9. Worthen AJ, Bagaria HG, Chen Y, Bryant SL, Huh C, Johnston KP. Nanoparticle-stabilized carbon dioxide-in-water foams with fine texture. *J Colloid Interface Sci*. 2013;391(0):142–151.
10. Adkins SS, Chen X, Chan I, Torino E, Nguyen QP, Sanders AW, Johnston KP. Morphology and stability of CO_2-in-water foams with nonionic hydrocarbon surfactants. *Langmuir*. 2010;26(8):5335–5348.
11. Eastoe J, Gold S, Steytler DC. Surfactants for CO_2. *Langmuir*. 2006;22(24):9832–9842.
12. Eastoe J, Paul A, Downer A, Steytler DC, Rumsey E. Effects of fluorocarbon surfactant chain structure on stability of water-in-carbon dioxide microemulsions. Links between Aqueous surface tension and microemulsion stability. *Langmuir*. 2002;18:3014–3017.
13. Lee CT Jr, Psathas PA, Ziegler KJ, Johnston KP, Dai HJ, Cochran HD, Melnichenko YB, Wignall GD. Formation of water-in-carbon dioxide microemulsions with a cationic surfactant: a small-angle neutron scattering study. *J Phys Chem B*. 2000;104(47):11094–11102.
14. Lee CT Jr, Psathas PA, Johnston KP, DeGrazia J, Randolph TW. Water-in-carbon dioxide emulsions: formation and stability. *Langmuir*. 1999;15(20):6781–6791.
15. Johnston KP, Cho D, da Rocha SRP, Psathas PA, Ryoo W, Webber SE, Eastoe J, Dupont A, Steytler DC. Water in carbon dioxide macroemulsions and miniemulsions with a hydrocarbon surfactant. *Langmuir*. 2001;17:7191–7193.
16. da Rocha SRP, Dickson JL, Cho D, Rossky PJ, Johnston KP. Stubby surfactants for the stabilization of water and CO_2 emulsions: Trisiloxanes. *Langmuir*. 2003;19:3114–3120.
17. Xing D, Wei B, Trickett K, Mohamed A, Eastoe J, Soong Y, Enick RM. CO_2-soluble surfactants for improved mobility control. In: SPE 129907, Presented at SPE Improved Oil Recovery Symposium, April 24–28, 2010, Tulsa, OK.
18. da Rocha SRP, Psathas PA, Klein E, Johnston KP. Concentrated CO_2-in-water emulsions with nonionic polymeric surfactants. *J Colloid Interface Sci*. 2001;239(1):241–253.
19. McLendon WJ, Koronaios P, McNulty S, Enick RM, Biesmans G, Miller A, Salazar L, Soong Y, Romanov V, Crandall D. Assessment of CO_2-soluble surfactants for mobility reduction using mobility measurments and CT imaging. In: SPE 154205, Presented at SPE Improved Oil Recovery Symposium, April 14–18, 2012, Tulsa, OK.
20. Lee HO, Heller JP. Laboratory measurements of CO_2-foam mobility. *SPE Reservoir Eng*. 1990;5(2):193–197.
21. Kuhlman MI, Falls AH, Hara SK, Monger-McClure TG, Borchardt JK. CO_2 foam with surfactants used below their critical micelle concentrations. *SPE Reservoir Eng*. 1992;7(4):445–452.
22. Kutay SM, Schramm LL. Structure/Performance relationships for surfactant and polymer stabilized foams in porous media. *J Can Pet Technol*. 2004;43(2):19–28.
23. Espinosa D, Caldelas F, Johnston KP, Bryant SL, Huh C. Nanoparticle-stabilized supercritical CO_2 foams for potential mobility control applications. SPE 129925, Presented at SPE Improved Oil Recovery Symposium, April 26–28, 2010, Tulsa, OK.
24. Dickson JL, Binks BP, Johnston KP. Stabilization of carbon dioxide-in-water emulsions using silica particles. *Langmuir*. 2004;20:7976–7983.
25. Aveyard R, Binks BP, Clint JH. Emulsions stabilised solely by colloidal particles. *Adv Colloid Interface Sci*. 2003;100-102:503–546.
26. Golomb D, Barry E, Ryan D, Swett P, Duan H. Macroemulsions of liquid and supercritical CO_2-in-water and water-in-liquid CO_2 stabilized by fine particles. *Ind Eng Chem Res*. 2006;45(8):2728–2733.
27. Binks BP. Particles as surfactants – similarities and differences. *Curr Opin Colloid Interface Sci*. 2002;7:21–41.
28. Cui ZG, Cui CF, Zhu Y, Binks BP. Multiple phase inversion of emulsions stabilized by in situ surface activation of $CaCO_3$ nanoparticles via adsorption of fatty acids. *Langmuir*. 2012;28(1):314–320.
29. Hunter TN, Wanless EJ, Jameson GJ, Pugh RJ. Non-ionic surfactant interactions with hydrophobic nanoparticles: impact on foam stability. *Colloids Surf A: Physicochem Eng Aspects*. 2009;347(1–3):81–89.
30. Dickson JL, Gupta G, Horozov TS, Binks BP, Johnston KP. Wetting phenomena at the CO_2/water/glass interface. *Langmuir*. 2006;22(5):2161–2170.
31. Vignati E, Piazza R, Lockhart TP. Pickering emulsions: interfacial tension, colloidal layer morphology, and trapped-particle motion. *Langmuir*. 2003;19(17):6650–6656.
32. Binks BP, Rodrigues JA, Frith WJ. Synergistic interaction in emulsions stabilized by a mixture of silica nanoparticles and cationic surfactant. *Langmuir*. 2007;23(7):3626–3636.
33. Lan Q, Yang F, Zhang S, Liu S, Xu J, Sun D. Synergistic effect of silica nanoparticle and cetyltrimethyl ammonium bromide on the stabilization of O/W emulsions. *Colloids Surf A: Physicochem Eng Aspects*. 2007;302(1–3):126–135.
34. Ravera F, Ferrari M, Liggieri L, Loglio G, Santini E, Zanobini A. Liquid–liquid interfacial properties of mixed nanoparticle–surfactant systems. *Colloids Surf A: Physicochem Eng Aspects*. 2008;323(1–3):99–108.
35. Binks BP, Rodrigues JA. Double inversion of emulsions by using nanoparticles and a di-chain surfactant. *Angewandte Chemie*. 2007;119(28):5485–5488.
36. Cui ZG, Cui YZ, Cui CF, Chen Z, Binks BP. Aqueous foams stabilized by in situ surface activation of $CaCO_3$ nanoparticles via adsorption of anionic surfactant. *Langmuir*. 2010;26(15):12567–12574.
37. Akartuna I, Studart AR, Tervoort E, Gonzenbach UT, Gauckler LJ. Stabilization of oil-in-water emulsions by colloidal particles modified with short amphiphiles. *Langmuir*. 2008;24(14):7161–7168.
38. Binks BP, Rodrigues JA. Enhanced stabilization of emulsions due to surfactant-induced nanoparticle flocculation. *Langmuir*. 2007;23(14):7436–7439.
39. Jiang T, Hirasaki GJ, Miller CA, Ng S. Wettability alteration of clay in solid-stabilized emulsions. *Energy Fuels*. 2011;25(6):2551–2558.
40. Partyka S, Lindheimer M, Faucompre B. Aggregate formation at the solid–liquid interface: the calorimetric evidence. *Colloids Surf A: Physicochem Eng Aspects*. 1993;76:267–281.
41. Mannhardt K, Schramm LL, Novosad JJ. Effect of rock type and brine composition on adsorption of two foam-forming surfactants *SPE Adv Technol Ser*. 1993;1(1):212–218.
42. Mannhardt K, Novosad JJ, Jha KN. Adsorption of foam-forming surfactants in Berea sandstone. *J Can Pet Technol*. 1994;33(2):34–43.
43. Lv W, Bazin B, Ma D, Liu Q, Han D, Wu K. Static and dynamic adsorption of anionic and amphoteric surfactants with and without the presence of alkali. *J Pet Sci Eng*. 2011;77(2):209–218.

44. Levinson MI. Surfactant production: present realities and future perspectives. In: Zoller U, Sosis P, editors. Handbook of Detergents Part F: Production. Boca Raton, FL: Taylor & Francis Group, LLC, 2009:1–36.
45. Chen X, Adkins SS, Nguyen QP, Sanders AW, Johnston KP. Interfacial tension and the behavior of microemulsions and macroemulsions of water and carbon dioxide with a branched hydrocarbon nonionic surfactant. *J Supercrit Fluids*. 2010;55(2):712–723.
46. Johansson A, Kollman P, Rothenberg S, McKelvey J. Hydrogen bonding ability of the amide group. *J Am Chem Soc*. 1974;96(12):3794–3800.
47. Lomax EG, editor. Amphoteric Surfactants, 2nd ed. New York: Marcel Dekker, 1996. Surfactant Science Series.
48. Holmes JD, Ziegler KJ, Audriani M, Lee Jr. CT, Bhargava PA, Steytler DC, Johnston KP. Buffering the aqueous phase pH in water-in-CO_2 microemulsions. *J Phys Chem B*. 1999;103:5703–5711.
49. Yoon KY, Li Z, Neilson BM, Lee W, Huh C, Bryant SL, Bielawski CW, Johnston KP. Effect of adsorbed amphiphilic copolymers on the interfacial activity of superparamagnetic nanoclusters and the emulsification of oil in water. *Macromolecules*. 2012;45(12):5157–5166.
50. Saleh N, Sarbu T, Sirk K, Lowry GV, Matyjaszewski K, Tilton RD. Oil-in-water emulsions stabilized by highly charged polyelectrolyte-grafted silica nanoparticles. *Langmuir*. 2005;21(22):9873–9878.
51. Saigal T, Dong H, Matyjaszewski K, Tilton RD. Pickering emulsions stabilized by nanoparticles with thermally responsive grafted polymer brushes. *Langmuir*. 2010;26(19):15200–15209.
52. Binks BP, Murakami R. Phase inversion of particle-stabilized materials from foams to dry water. *Nat Mater*. 2006;5(11):865–869.
53. Hunter TN, Pugh RJ, Franks GV, Jameson GJ. The role of particles in stabilising foams and emulsions. *Adv Colloid Interface Sci*. 2008;137(2):57–81.
54. Binks BP, Kirkland M, Rodrigues JA. Origin of stabilisation of aqueous foams in nanoparticle-surfactant mixtures. *Soft Matter*. 2008;4(12):2373–2382.
55. Binks BP, Clint JH. Solid wettability from surface energy components: relevance to pickering emulsions. *Langmuir*. 2002;18:1270–1273.
56. Walstra P, Smulders PEA. Emulsion formation. In: Binks BP, editor. Modern Aspects of Emulsion Technology. Cambridge: The Royal Society of Chemistry, 1998:56–99.
57. Otsubo Y, Prud'homme RK. Rheology of oil-in-water emulsions. *Rheologica Acta*. 1994;33(1):29–37.
58. Hirasaki GJ, Lawson JB. Mechanisms of foam flow in porous media: apparent viscosity in smooth capillaries. *Soc Pet Eng J*. 1985:176–190.
59. Pal R. Effect of droplet size on the rheology of emulsions. *AIChE J*. 1996;42(11):3181–3190.
60. Falls AH, Musters JJ, Ratulowski J. The apparent viscosity of foams in homogeneous bead packs. *SPE Reservoir Eng*. 1989;4(55):155–164.
61. Alvarez JM, Rivas HJ, Rossen WR. Unified model for steady-state foam behavior at high and low foam qualities. *SPE J*. 2001;6(3):325–333.
62. Midmore BR. Preparation of a novel silica-stabilized oil/water emulsion. *Colloids Surf A: Physicochem Eng Aspects*. 1998;132 (2–3):257–265.
63. Derjaguin BV, Churaev NV. Structural component of disjoining pressure. *J Colloid Interface Sci*. 1974;49(2):249–255.
64. Aronson AS, Bergeron V, Fagan ME, Radke CJ. The influence of disjoining pressure on foam stability and flow in porous media. *Colloids Surf A: Physicochem Eng Aspects*. 1994;83(2):109–120.
65. Stubenrauch C, von Klitzing R. Disjoining pressure in thin liquid foam and emulsion films-new concepts and perspectives. *J Phys: Condens Matter*. 2003;15(27):R1197–R1232.
66. Aveyard R, Binks BP, Esquena J, Fletcher PDI, Bault P, Villa P. Flocculation transitions of weakly charged oil-in-water emulsions stabilized by different surfactants. *Langmuir*. 2002;18(9):3487–3494.
67. Chengara A, Nikolov AD, Wasan DT, Trokhymchuk A, Henderson D. Spreading of nanofluids driven by the structural disjoining pressure gradient. *J Colloid Interface Sci*. 2004;280(1):192–201.
68. Wasan D, Nikolov A. Thin liquid films containing micelles or nanoparticles. *Curr Opin Colloid Interface Sci*. 2008;13(3):128–133.
69. Langevin D. Influence of interfacial rheology on foam and emulsion properties. *Adv Colloid Interface Sci*. 2000;88(1,2):209–222.
70. Lucassen-Reynders EH, Cagna A, Lucassen J. Gibbs elasticity, surface dilational modulus and diffusional relaxation in nonionic surfactant monolayers. *Colloids Surf A: Physicochem Eng Aspects*. 2001;186(1–2):63–72.
71. Wasan DT, Gupta L, Vora MK. Interfacial shear viscosity at fluid-fluid interfaces. *AIChE J*. 1971;17(6):1287–1295.
72. Lishchuk SV, Halliday I. Effective surface viscosities of a particle-laden fluid interface. *Phys Rev E*. 2009;80(1):016306.
73. Murray BS, Durga K, Yusoff A, Stoyanov SD. Stabilization of foams and emulsions by mixtures of surface active food-grade particles and proteins. *Food Hydrocolloids*. 2011;25(4):627–638.
74. Wijmans CM, Dickinson E. Simulation of interfacial shear and dilatational rheology of an adsorbed protein monolayer modeled as a network of spherical particles. *Langmuir*. 1998;14(25):7278–7286.
75. Pugh RJ. Experimental techniques for studying the structure of foams and froths. *Adv Colloid Interface Sci*. 2005;114–115:239–251.
76. Kabalnov A, Wennerstrom H. Macroemulsion Stability: the oriented wedge theory revisited. *Langmuir*. 1996;12:276–292.
77. Vrij A, Overbeek JTG. Rupture of thin liquid films due to spontaneous fluctuations in thickness. *J Am Chem Soc*. 1968;90(12):3074–3078.
78. Babak VG, Stebe M-J. Highly concentrated emulsions: physicochemical principles of formulation. *J Dispersion Sci Technol*. 2002;23 (1–3):1–22.

Manuscript received Dec. 19, 2012, and revision received Apr. 1, 2013.